Ocean Modelling 66 (2013) 64–76

Contents lists available at SciVerse ScienceDirect

Ocean Modelling

journal homepage: www.elsevier.com/locate/ocemod

Impact of uncertainties in the horizontal density gradient upon low resolution global ocean modelling

Jean-Michel Brankart

CNRS/Univ. Grenoble 1, Laboratoire de Glaciologie et Géophysique de l'Environnement (LGGE) UMR 5183, Grenoble, F-38041, France

ARTICLE INFO

Article history:
Received 13 September 2012
Received in revised form 6 February 2013
Accepted 9 February 2013
Available online 14 March 2013

Keywords:
Model uncertainties
Stochastic parameterization
Equation of state
Global ocean model

ABSTRACT

In this study, it is shown (i) that, as a result of the nonlinearity of the seawater equation of state, unresolved scales represent a major source of uncertainties in the computation of the large-scale horizontal density gradient from the large-scale temperature and salinity fields, and (ii) that the effect of these uncertainties can be simulated using random processes to represent unresolved temperature and salinity fluctuations. The results of experiments performed with a low resolution global ocean model show that this parameterization has a considerable effect on the average large-scale circulation of the ocean, especially in the regions of intense mesoscale activity. The large-scale flow is less geostrophic, with more intense associated vertical velocities, and the average geographical position of the main temperature and salinity fronts is more consistent with observations. In particular, the simulations suggest that the stochastic effect of the unresolved temperature and salinity fluctuations on the large-scale density field may be sufficient to explain why the Gulf Stream pathway systematically overshoots in non-stochastic low resolution ocean models.

1. Introduction

One of the most salient feature of today's state-of-the-art ocean models is that they are essentially *deterministic* models, in the sense that they do not involve *random numbers* to represent uncertainties in the model equations, parameters and forcing, or to simulate the effect of unresolved processes. Yet, this deterministic model dynamics is known to become chaotic as soon as mesoscale eddies are resolved by the model, so that the simulated mesoscale flow can only be viewed as one random realization sampled from a large set of possibilities. It is thus only in a statistical sense that the mesoscale can be compared to the real world, and it is only as a stochastic process that the effect of the mesoscale in the model can be analysed. Mesoscale fluctuations indeed produce a considerable effect on the general circulation of the ocean (Zhai et al., 2004; Penduff et al., 2010), with prominent contributions to momentum, heat and salt fluxes, which cannot be easily parameterized in low resolution models.

As a general rule, the effect of uncertainties or unresolved processes (even if unbiased) does not average to zero in a nonlinear model. For instance, if the wind is fluctuating or if it is uncertain, then neglecting the fluctuations or the uncertainties systematically underestimates the air–sea momentum flux (proportional to the square of the wind speed). In the same way, the average effect of the mesoscale fluctuations does not vanish in the two nonlinear terms of the primitive equations: the advection term and the equation of state. Concerning the advection term, this effect was originally parameterized in ocean models using empirically specified horizontal diffusion (Bryan et al., 1979), and afterwards using more and more sophisticated advection/diffusion operators (see Griffies et al., 2000 for a review). Concerning the equation of state, the effect of the mesoscale temperature and salinity fluctuations on the large-scale density field is generally ignored, maybe because it cannot be easily parameterized using a deterministic formulation. However, it can easily be argued (see Section 3.1), that, in low resolution ocean models, the resulting approximation in the large-scale density is a major source of uncertainties in the horizontal pressure gradient, and thus in the horizontal momentum balance equation.

A different point of view can also be adopted to deal with model uncertainties. Rather than parameterizing their mean effect in the model, they can be explicitly simulated by including a random forcing in the model equations. This can be done to produce ensemble forecasts (Buizza et al., 1999; Palmer et al., 2005) or to simulate model error in ensemble data assimilation methods (Evensen, 1994). In such applications, the random forcing is not only responsible for the dispersion of the ensemble; it can also produce a significant mean effect in the simulations (Berner et al., in press; Williams, 2012; Palmer, 2012). In this study, the same kind of approach is used to simulate the uncertainties that unresolved mesoscale temperature and salinity fluctuations produce on the

E-mail address: Jean-Michel.Brankart@hmg.inpg.fr

1463-5003/$ - see front matter © 2013 Elsevier Ltd. All rights reserved.
http://dx.doi.org/10.1016/j.ocemod.2013.02.004

large-scale horizontal density field. The objective is to propose a simple (empirically specified) stochastic parameterization of these uncertainties (in Section 3), and to evaluate the impact that this parameterization may have on the ocean circulation (in Section 4), as simulated by a low resolution global model configuration (described in Section 2).

2. A low resolution global ocean model

The purpose of this section is to present the NEMO primitive equation model and to describe the ORCA2 low resolution global ocean configuration.

2.1. The NEMO primitive equation model

The ocean general circulation model that is used in this study is the NEMO model (Nucleus for European Modelling of the Ocean), as described in Madec (2008). The model approximates the ocean circulation by the primitive equations:

- the momentum balance equation:

$$\frac{\partial \mathbf{U}_h}{\partial t} = -\left[(\nabla \times \mathbf{U}) \times \mathbf{U} + \frac{1}{2}\nabla(\mathbf{U}^2)\right] - f\mathbf{k} \times \mathbf{U}_h - \frac{1}{\rho_0}\nabla_h p + \mathbf{D}^U + \mathbf{F}^U \tag{1}$$

where t is time; $\mathbf{k}$, the local upward unit vector; $\mathbf{U}$, the velocity vector ($\mathbf{U}_h$ is the horizontal component, orthogonal to $\mathbf{k}$, and w, the vertical velocity); p is pressure; ρ_0, a reference density; and $f = 2\mathbf{\Omega} \times \mathbf{k}$, the Coriolis acceleration (where $\mathbf{\Omega}$ is the Earth angular velocity);
- the hydrostatic equilibrium equation:

$$\frac{\partial p}{\partial z} = -\rho g \tag{2}$$

where z is the vertical coordinate (in the direction of $\mathbf{k}$); ρ is *in situ* density; and g, gravitational acceleration;
- the incompressibility equation:

$$\nabla \cdot \mathbf{U} = 0 \tag{3}$$

- the heat and salt conservation equations:

$$\frac{\partial T}{\partial t} = -\nabla \cdot (T\mathbf{U}) + D^T + F^T \tag{4}$$

$$\frac{\partial S}{\partial t} = -\nabla \cdot (S\mathbf{U}) + D^S + F^S \tag{5}$$

where T is potential temperature and S, salinity;
- the equation of state:

$$\rho = \rho[T, S, p_0(z)] \tag{6}$$

where $p_0(z) = \rho_0 g z$ is the reference pressure as a function of depth.

In these equations, $\mathbf{D}^U, D^T$ and D^S represent the parameterization of small-scale physics for momentum, temperature and salinity, and $\mathbf{F}^U, F^T$ and F^S are surface forcing terms.

These equations are complemented by boundary conditions, which are applied at the ocean bottom and at the interface with the atmosphere. Kinematic conditions consist in a 'no flow' condition across the ocean bottom:

$$w = -\mathbf{U}_h \cdot \nabla_h H \tag{7}$$

where H is ocean depth, and a prognostic equation for the sea surface height η:

$$\frac{\partial \eta}{\partial t} = -\nabla \cdot \left[(H + \eta)\overline{\mathbf{U}}_\mathbf{h}\right] + \mathbf{P} - \mathbf{E} \tag{8}$$

where $\overline{\mathbf{U}}_\mathbf{h}$ is the vertical average of horizontal velocity; P, precipitation; and E, evaporation. Dynamic boundary conditions parameterize the exchange of momentum and heat across the bottom and surface boundaries. Since they depend on the parameterization used for $\mathbf{D}^U$ and D^T, they will be described later in Section 2.2.

From Eqs. (2) and (8), it results that the horizontal pressure gradient $\nabla_h p$ in Eq. (1) is given by:

$$\nabla_h p = \nabla_h p_s + \int_{\zeta=z}^{\zeta=0} g \nabla_h \rho d\zeta \tag{9}$$

where $p_s = \rho_s g \eta$ is the surface pressure gradient, and ρ_s is surface density. Thus the horizontal pressure gradient depends on the thermohaline structure of the ocean (T and S) through the equation of state in Eq. (6). In realistic applications of NEMO, the equation of state is the standard empirical equation defined by the Joint Panel on Oceanographic Tables and Standards (UNESCO, 1983), in a version that has been reformulated by Jackett and McDougall (1995) (by a modification of the coefficients of the K polynomial in the equation below), to allow direct computation of *in situ* density from potential temperature (rather than *in situ* temperature):

$$\rho(T, S, p) = \frac{\rho(T, S, 0)}{1 - p/K(T, S, p)} \tag{10}$$

where $\rho(T, S, 0)$ is a 15-term polynomial in T and S; and $K(T, S, p)$, a 26-term polynomial in T, S and p. One of the main characteristics of the seawater equation of state is thus to be quite nonlinear (see Fig. 1). In addition, it must be remembered that, in principle, it is only valid for a fluid parcel in thermodynamic equilibrium.

2.2. The ORCA2 configuration

The NEMO configuration used in this study is the ORCA2 configuration, as described in Madec and Imbard (1996). It is a low resolution configuration, which is provided with the model code (<http://www.nemo-ocean.eu/>), and which is used here exactly

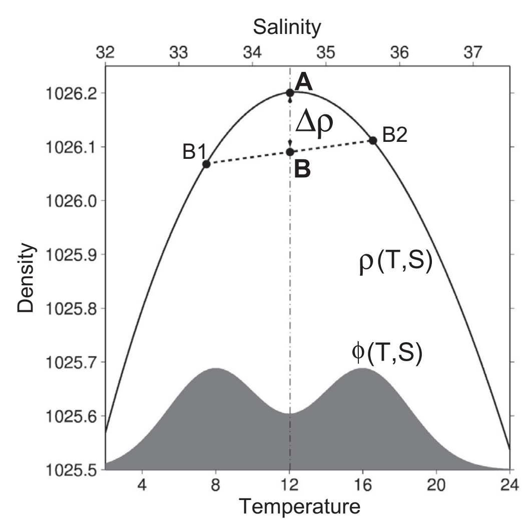

Fig. 1. Sea water equation of state (thick solid line) for joint temperature and salinity variations between 2 °C and 24 °C (bottom axis) and 32 and 37.5 (top axis) respectively. A typical distribution of unresolved temperature and salinity fluctuations is represented by the grey histogram, which superposes two Gaussian distributions with means at $T = 8$ °C, $S = 33.5$ and $T = 16$ °C, $S = 35.5$, and identical standard deviations: $\sigma_T = 2.5$ °C, $\sigma_S = 0.625$. The density at point A is computed by applying the equation of state to the mean of the distribution: $T = 12$ °C and $S = 34.5$, whereas the density at point B takes into account the distribution of unresolved temperature and salinity fluctuations. Points B1 and B2 show that the same density can be obtained as the mean of two densities obtained from opposite temperature and salinity fluctuations.

as distributed in the version 3.3 of NEMO (except that full steps are used instead of partial steps to discretize bottom topography, see below). See Table 1 for a summary of the main model parameters.

ORCA2 numerics. In this configuration, the NEMO model Eqs. (1) to (6) are discretized using an ORCA type horizontal grid, with a horizontal resolution of $2^\circ \times 2^\circ$ (reduced to a meridional grid spacing of $1/2^\circ$ in tropical regions), and 31 z-coordinate levels along the vertical (from 10 m resolution in the first 120 m to 500 m resolution for the last levels). The bottom boundary is discretized using full steps of the vertical grid, so that the discretization of Eq. (9) for the horizontal pressure gradient remains straightforward down to the bottom, without vertical re-interpolation of T and S in the partial step to obtain the last level density gradient (see Barnier et al., 2006 for more details about partial steps). On the other hand, the time derivatives in Eqs. (1), (4), (5) and (8) are discretized using a leap-frog scheme, with a time step $\Delta t = 5760$s (15 time steps per day).

ORCA2 physics. This discretization of the equations is designed to resolve the large-scale component of the ocean circulation, while the effect of small-scale physics is parameterized in Eqs. (1), (4) and (5) by diffusion operators in $\mathbf{D}^U, D^T$ and D^S. Lateral diffusion of momentum and tracers is obtained by an iso-neutral Laplacian operator, with specified viscosities and diffusivities (see Table 1), which is complemented at the lateral boundaries by a condition of no heat and salt fluxes for Eqs. (4) and (5) and by a condition of no slip for Eq. (1). Vertical diffusion of momentum and tracers is obtained by a turbulent closure scheme based on a prognostic equation for turbulent kinetic energy and a closure assumption for turbulent length scales, see Blanke and Delecluse, 1993, which is complemented, at the bottom boundary, by a parameterization of bottom friction (momentum flux) and geothermal heating (heat flux), and at the surface boundary, by a parameterization of air–sea fluxes. In addition to this subgrid scale parameterization, an additional term is introduced in the momentum balance Eq. (1) to damp the fast external gravity waves (see Roullet and Madec, 2000 for more details). This parameterization can be interpreted as a diffusion of the vertically integrated volume flux divergence (first term in the right hand side of Eq. 8), which is designed in such a way that the faster external gravity waves no longer propagate (so that the above time step is also sufficient to resolve the external mode).

ORCA2 initial condition and forcing. The two model simulations described in this paper are started from rest ($\mathbf{U} = 0, \eta = 0$), and from climatological temperature and salinity fields corresponding to the January climatology from the World Ocean Database, Levitus et al., 1998. The atmospheric forcing is computed using the CORE bulk parameterization (Large and Yeager, 2009) and climatological atmospheric data (see Table 1 for more details). The same atmospheric conditions are thus applied from year to year in a perpetual way.

Table 1
Main model parameters for the ORCA2 configuration (see Madec, 2008 for more details about the formulation of the numerical schemes).

ORCA2 numerics	
Horizontal resolution	$2^\circ \times 2^\circ$, reduced to $2^\circ \times 1/2^\circ$ in tropical regions
Vertical resolution	31 z-levels (from 10 m to 500 m vertical resolution)
Bathymetry discretization	Full steps approximation
Momentum advection	Vector form, energy and enstrophy conserving
Tracer advection	Total variance dissipation (TVD) scheme
Time stepping scheme	Leap frog, with Asselin filter ($\gamma = 0.1$)
Time step	$\Delta t = 5760$s (for internal and external modes, see text)
ORCA2 physics	
Lateral viscosity	$\nu = 40,000$ m^2/s (horizontal), smaller in the tropics
Lateral diffusivity	$\lambda = 2000$ m^2/s (iso-neutral), smaller in the tropics
Bottom boundary layer	Diffusive parameterization, with $\lambda_{bbl} = 1000$ m^2/s
TKE parameterization	As in Madec and Imbard (1996)
Additional mixing options	Double diffusive and tidal mixing parameterizations
ORCA2 initial and boundary conditions	
Initial condition	January climatology from the World Ocean Database
Bottom friction	Linear friction, with coefficient $r = 4 \times 10^{-4}$
Geothermal heating	As in Emile-Geay and Madec (2009)
Atmospheric forcing formulation	CORE bulk formulas (Large and Yeager, 2009)
Atmospheric data	10 m wind, air temperature and humidity (6-hourly) incoming short wave and long wave radiation (daily) total precipitation (monthly)
Surface salinity restoring	To Levitus climatology (with $\gamma_s = -166.67$ mm/day).
River runoffs	Monthly climatology, from the CORE database.

3. Uncertainties in the horizontal density gradient

As mentioned in Section 2.2, in a low resolution ocean model, the primitive Eqs. (1)–(6) are used to describe the large-scale component of the ocean circulation. In the averaging of the equations to extract the large scales, the effect of unresolved scales does not cancel out in the nonlinear terms of the equations, which are (i) the advection terms (first term in the right hand side of Eqs. (1), (4) and (5)), and (ii) the equation of state (Eq. (6), with the formulation given by Eq. (10)). In the advection terms, unresolved scales are assumed to produce an additional diffusion, which is parameterized by $\mathbf{D}^U, D^T$ and D^S (see Section 2.2). In the equation of state, the effect of unresolved scales is generally neglected, which means that the large-scale density ρ is computed from the large-scale potential temperature T and salinity S using the equilibrium formulation of the equation of state given by Eq. (10). Through the thermal wind Eq. (9), this approximation generates uncertainties in the relation between the large-scale thermohaline structure of the ocean (as obtained from Eq. (4) and (5)) and the large-scale horizontal pressure gradient, which is known to be one of the dominant terms in the momentum balance equation (Eq. (1)). The remaining of this paper is dedicated (i) to quantifying the importance of this approximation (in Section 3.1), (ii) to proposing a parameterization of the resulting uncertainty in the large-scale density (in Section (3.2), and (iii) to evaluating the impact of this uncertainty on the model circulation (in Section 4).

3.1. Effect of the unresolved scales on the large-scale density

The effect that unresolved mesoscale fluctuations produce in the computation of the large-scale density gradient has already been discussed in Appendix B of two papers by McDougall and McIntosh (1996), McDougall and McIntosh (2001). In the first one, the authors estimate that the error produced by unresolved temperature fluctuations of 1 °C can be 3% of the typical mean density gradient. Furthermore, they also show that this error is proportional to the mean square of unresolved temperature fluctuations (Eq. (B3) in McDougall and McIntosh (1996) or Eq. (19) below). This means that the effect is 100 times larger for unresolved temperature fluctuations of 10 °C (more typical of the Gulf Stream front). In addition, as will be shown below, the effect is also significantly amplified if there is a density maximum close to the middle of the front, which can happen if temperature and salinity variations across the front have an opposite effect on density (as in the Gulf Stream front). This can be related to the cabbeling process (e.g. Klocker and McDougall, 2010), by which denser water is produced by mixing two types of water of equal density but with different temperature and salinity (and which leads to the sinking of the resulting denser water). In a similar way, if density is computed from average (large-scale) temperature and salinity (as in all standard ocean models), then it is quite systematically larger than the (correct) average density (which should be used in the large-scale thermal wind Eq. (9)). This is like a spurious 'artificial cabbelling' that should be avoided to write consistent equations for the large-scale flow. To quantify the magnitude of this effect, the first thing to do is thus to introduce a mathematical description of the averaging (or filtering) operator extracting the large-scale component of the ocean circulation, and then to compute the density misfit that is produced if this filtering operator is applied after rather than before the equation of state.

(a) *Impact of averaging temperature and salinity on density*. If $\psi(\mathbf{x},\mathbf{x}')$ denotes the averaging operator (where $\mathbf{x}$ and $\mathbf{x}'$ are spatial coordinates), and if $T'(\mathbf{x}), S'(\mathbf{x})$ are the unresolved fluctuations of potential temperature and salinity, then the large-scale density $\rho(\mathbf{x})$ can be written:

$$\rho(\mathbf{x}) = \int \rho\left[T(\mathbf{x}') + T'(\mathbf{x}'), S(\mathbf{x}') + S'(\mathbf{x}'), p_0(z)\right]\psi(\mathbf{x},\mathbf{x}')d\mathbf{x}' \qquad (11)$$

This corresponds to replacing the assumption that the large-scale fluid parcel is in equilibrium (which is made in Eq. (6) by applying the equation of state to the large scale) by the assumption of local equilibrium (by applying the equation of state locally). This is clearly still an assumption, but it is the standard assumption that is made to apply equilibrium thermodynamics to fluid mechanics. Furthermore, it must be noted that the two assumptions would produce the same result if the equation of state was linear, since by definition of the averaging operator:

$$\int \left[T(\mathbf{x}') + T'(\mathbf{x}')\right]\psi(\mathbf{x},\mathbf{x}')d\mathbf{x}' = T(\mathbf{x}) \quad \text{and}$$
$$\int \left[S(\mathbf{x}') + S'(\mathbf{x}')\right]\psi(\mathbf{x},\mathbf{x}')d\mathbf{x}' = S(\mathbf{x}) \qquad (12)$$

The spatial integral in Eq. (11) can be transformed into an integral on temperature and salinity fluctuations (considered as random variables: δT and δS):

$$\rho(\mathbf{x}) = \int \rho[T(\mathbf{x}) + \delta T, S(\mathbf{x}) + \delta S, p_0(z)]\phi(\delta T, \delta S; \mathbf{x})\, d\delta T\, d\delta S \qquad (13)$$

where $\phi(\delta T, \delta S; \mathbf{x})$ is the distribution of temperature and salinity fluctuations (due to unresolved scales) corresponding to location $\mathbf{x}$:

$$\phi(\delta T, \delta S; \mathbf{x}) = \int \delta\left[T'(\mathbf{x}') - \delta T, S'(\mathbf{x}') - \delta S\right]\psi(\mathbf{x},\mathbf{x}')\, d\mathbf{x}' \qquad (14)$$

With the Dirac delta function δ, this last expression cumulates all temperature and salinity fluctuations ($T'(\mathbf{x}')$ and $S'(\mathbf{x}')$ in the neighbourhood of $\mathbf{x}$) that are equal to δT and δS. To each of them, it gives the weight $\psi(\mathbf{x},\mathbf{x}')$ depending on its spatial location with respect to $\mathbf{x}$, so that the distribution $\phi(\delta T, \delta S; \mathbf{x})$ integrates to 1 for every specified $\mathbf{x}$ [just as the averaging operator $\psi(\mathbf{x},\mathbf{x}')$]. Furthermore, as a direct consequence of Eq. (12), the mean of the distribution is $\delta T = 0$ and $\delta S = 0$.

To illustrate the effect that the distribution $\phi(\delta T, \delta S; \mathbf{x})$ of unresolved temperature and salinity fluctuations may have on the large-scale density, Fig. 1 shows the example of a temperature and salinity distribution typical of the Gulf Stream front (grey histogram along the T-axis in abcsissa). Along the front, two kinds of surface waters are assumed simultaneously present in the unresolved scales: cold and fresh waters on the one hand (with a mean at $T = 8\,^\circ\mathrm{C}$, $S = 33.5$), and warm and salty waters on the other hand (with a mean at $T = 16\,^\circ\mathrm{C}$, $S = 35.5$), both assumed with Gaussian temperature and salinity fluctuations. The thick solid curve shows the equilibrium equation of state (at the ocean surface: $z = 0$), as given by Eq. (10), which produces a maximum density close to $T = 12\,^\circ\mathrm{C}$ and $S = 34.5$. The density at point A is computed by applying the equation of state to the large-scale temperature (i.e. the mean of the distribution: $T = 12\,^\circ\mathrm{C}$ and $S = 34.5$) as in Eq. (6): $\rho^A = 1026.20\ \mathrm{kg/m^3}$, and the density at point B is computed by taking into account the distribution of unresolved temperature and salinity fluctuations (given by $\phi(\delta T, \delta S; \mathbf{x})$) using Eq. (13): $\rho^B = 1026.08\ \mathrm{kg/m^3}$. In realistic conditions, the curvature of the equation of state is most often negative, in which case the difference $\Delta\rho = \rho^B - \rho^A$ is *systematically* negative, and can only approach zero if the equation of state is close to linear in the range of the fluctuations. In this example case, the difference $\Delta\rho = -0.12\ \mathrm{kg/m^3}$ is far from negligible, but it is certainly important to get a better idea of the importance of this effect in the real ocean.

(b) *Estimation of $\Delta\rho$ from reanalysis data.* For that purpose, it is necessary to use a gridded ocean data set with both temperature and salinity at sufficient horizontal resolution. One possible product is the GLORYS global ocean reanalysis dataset (Ferry et al., 2010), which is produced by Mercator-Ocean by assimilating all available ocean observations (such as satellite altimetric data, sea surface temperature, ARGO floats,...) in a $1/4^\circ$ resolution global configuration of the NEMO model (the ORCA025 configuration, as developed by The DRAKKAR Group (2007)). Thus the smaller wavelength that can be represented by the ORCA2 grid corresponds to about 16 grid points in the GLORYS reanalysis, which can be expected to contain a significant part of the signal that is not resolved by the ORCA2 configuration. A *lower bound* for $|\Delta\rho|$ can thus be obtained by computing ρ^A from the 16×16 block-mean potential temperature and salinity, and ρ^B as the 16×16 block-mean density. In the above formalism, this corresponds to using the block-mean operator as a proxy for the averaging operator in Eq. (11), which means identifying the unresolved scales to all wavelengths below two ORCA2 grid points that are present in the GLORYS reanalysis.

Fig. 2 shows the resulting estimate of $\Delta\rho$ that is obtained (a) for the surface model layer on January 1, 2009 (top panel), (b) for the vertical profile at 47.5°W 42.6°N for the same date (bottom left panel), and (c) for the 2009 surface time series at the same horizontal location (bottom right panel). What can be observed in this figure is first that the effect of unresolved scales on the large-scale density is mainly concentrated in the Western boundary currents and in the Antarctic circumpolar current, because it is in these regions that the mesoscale activity is the most intense. The effect is especially strong along the Northern edge of the Gulf Stream front, because in addition to the intense mesoscale activity and the sharp temperature and salinity gradients, the equation of state produces a maximum density close to the middle of the current (as illustrated in Fig. 1). Second, as a result of the vertical coherence of the mesoscale temperature and salinity fluctuations, $\Delta\rho$ is only smoothly varying with depth, first in the mixed layer (down to 200 m depth in the winter example of Fig. 2), and then slowly decreasing in the deep thermocline (down to about 1000 m depth). In the Gulf Stream region, the vertical average of $\Delta\rho$ over the first 1000 m can typically reach 0.1 $\mathrm{kg/m^3}$ (corresponding to a pressure difference of about 0.1 m), which is thus far from being negligible. Third, as illustrated by the time series in Fig. 2, $\Delta\rho$ is fluctuating in time in relation to the modification of the pattern of the unresolved scales (which mainly results, in Fig. 2, from the movement of mesoscale eddies). In the horizontal map (top panel of Fig. 2), these fluctuations look smooth on the horizontal because $\Delta\rho$ is shown at the $1/4^\circ$ resolution of the GLORYS reanalysis (using a boxcar filter). If the resolution is degraded to the ORCA2 resolution, it can be observed, on the contrary, that these high-frequency fluctuations are mostly decorrelated from one ORCA2 grid point to the next. In addition, the time series shows a seasonal cycle: $|\Delta\rho|$ is smaller during summer because temperature is higher, so that the nonlinearity of the equation of state does not produce the same effect.

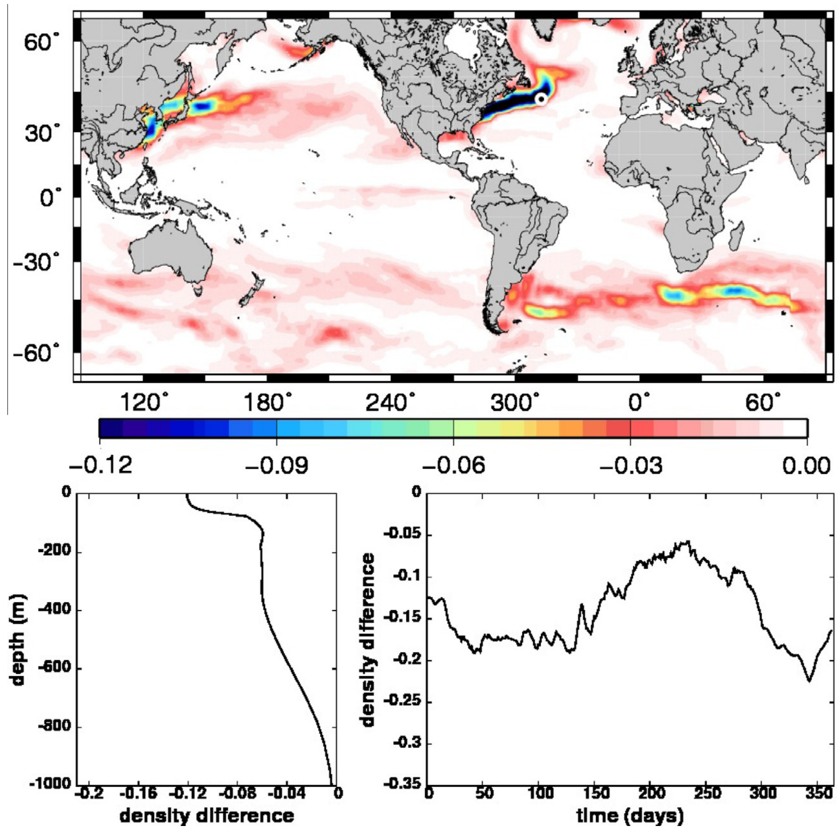

Fig. 2. Estimate of $\Delta\rho$ computed from the GLORYS ocean reanalysis (a) for the surface model layer on January 1, 2009 (top panel), (b) for the vertical profile at 47.5°W 42.6°N (the position of the black dot in the top panel) for the same date (bottom left panel), and (c) for the 2009 surface time series at the same horizontal location (bottom right panel).

This summarizes the typical behaviour that can be expected for the effect of unresolved scales on the large-scale density field. The next step is to propose a parameterization that can reproduce the same kind of behaviour in a low resolution ocean model.

3.2. Stochastic equation of state

To parameterize Eq. (13), a first simplification is to replace the integral by the summation:

$$\rho = \frac{1}{2p}\sum_{i=1}^{p}\{\rho[T+\Delta T_i, S+\Delta S_i, p_0(z)] + \rho[T-\Delta T_i, S-\Delta S_i, p_0(z)]\} \tag{15}$$

where $\Delta T_i, \Delta S_i,\ i = 1,\ldots,p$ is a set of temperature and salinity fluctuations simulating the effect of the distribution ϕ in Eq. (13). The first thing to observe in this equation is that, whatever the fluctuations ΔT_i and ΔS_i, they will never affect density if the equation of state is linear (consistently with Eqs. (11) and (13)). It is very important that this basic property is embedded in the parameterization from the very beginning. The second thing to observe about Eq. (15) is that it contains no approximation: providing that the equation of state is convex, there is always a set of fluctuations $\Delta T_i, \Delta S_i,\ i = 1,\ldots,p$ (whatever $p \geqslant 1$) such that the summation in Eq. (15) is equal to the integral in Eq. (13). For instance, for $p = 1$, Fig. 1 shows the temperature and salinity fluctuations required to produce the same effect as the temperature and salinity distribution. The only reason for using $p > 1$ in Eq. (15) is to simplify the construction of a realistic model for the space and time dependence between the fluctuations. (ΔT_i and ΔS_i are indeed functions of $\mathbf{x}$ and t, even if this dependence was omitted in Eq. (15) for simplicity.)

The last step is then to provide a parameterization for the fluctuations ΔT_i and ΔS_i in Eq. (15). Since the unresolved scales are unknown by definition, and produce fluctuating uncertainties on the large-scale density (as observed in Fig. 2), a natural means of representing their effect in the low resolution model is to parameterize ΔT_i and ΔS_i as stochastic processes. To produce fluctuations ΔT_i and ΔS_i consistent with local dynamics, a simple solution is to use the temperature and salinity difference with respect to random walks ξ_i around the current grid point. Moreover, if the random walks ξ_i are designed to be small enough (typically a few model grid points), then the fluctuations can be computed simply by using the local gradient:

$$\Delta T_i = \xi_i \cdot \nabla T \quad \text{and} \quad \Delta S_i = \xi_i \cdot \nabla S \tag{16}$$

In this way, Eq. (15) can be interpreted as the mean density over $2p$ random walks surrounding each model grid point (with central symmetry of the $2p$ temperature and salinity fluctuations).

(a) *Stochastic processes.* To parameterize the random walks $\xi_i,\ i = 1,\ldots,p$ in Eq. (16), the most simple (non-degenerate) solution is to assume that the three components $\xi_{i,x}, \xi_{i,y}$ and $\xi_{i,z}$ of every ξ_i are *independent* first-order autoregressive processes (or Langevin processes), which can be obtained iteratively (from timestep t_{k-1} to timestep t_k) by the equation:

$$\begin{bmatrix} \xi_{i,x}(t_k) \\ \xi_{i,y}(t_k) \\ \xi_{i,z}(t_k) \end{bmatrix} = \varphi_i \begin{bmatrix} \xi_{i,x}(t_{k-1}) \\ \xi_{i,y}(t_{k-1}) \\ \xi_{i,z}(t_{k-1}) \end{bmatrix} + \sqrt{1-\varphi_i^2}\begin{bmatrix} w_{i,x} \\ w_{i,y} \\ w_{i,z} \end{bmatrix} \tag{17}$$

where the parameter $\varphi_i \leqslant 1$ is related to the decorrelation timescale τ_i (in timesteps) of each random walk by:

$$\varphi_i = \exp(-1/\tau_i) \tag{18}$$

and where $w_{i,x}, w_{i,y}$ and $w_{i,z}$ are here assumed to be *Gaussian* white noises, with zero mean and respective standard deviation $\ell_{i,x}, \ell_{i,y}$ and $\ell_{i,z}$. In this way, $\xi_{i,x}, \xi_{i,y}$ and $\xi_{i,z}$ remain Gaussian at any future time (since Eq. (17) is linear), with asymptotic standard deviations also equal to $\ell_{i,x}, \ell_{i,y}$ and $\ell_{i,z}$, respectively. Fig. 3 shows for instance 2 independent random walks as obtained using Eq. (17), with $\ell_{i,x} = \ell_{i,y} = 2$; grid points and $\tau_i = 180$; time steps. From a mathematical point of view, it is interesting to note that, in this stochastic parameterization, there can be no ambiguity between Itô and Stratonovich interpretations of delta-correlated random processes (see Van Kampen, 2007 chapter 9), except in the limit case of a zero correlation time scale [$\varphi_i = 0$] in Eq. (17): (i) in the equations for the random walks (17), the two formulations are equivalent since the delta-correlated (white) Gaussian noises $w_{i,x}, w_{i,y}, w_{i,z}$ appears as an additive noise, not as a multiplicative noise; (ii) in all other equations becoming stochastic (equation of state (15), thermal wind Eqs. (9), momentum balance Eqs. (1) and then Eqs. (3)–(5) as well), Itô's formulation cannot apply since the random processes are no more delta-correlated (except if $\varphi_i = 0$).

This idea that stochastic processes can represent mesoscale eddies is not new in the ocean literature (e.g. Berloff, 2005). The usual approach is to start from statistical mechanics considerations, and to derive a simplified statistical description of the mesoscale fluctuations. This has been done to obtain a variety of deterministic (as in Kazantsev et al. (1998)) or stochastic (as in Zidikheri and Frederiksen (2010)) parameterizations of mesoscale turbulence (see Frederiksen et al., 2012 for a review). These studies are useful to improve the statistics of the fluctuations, but they are mostly theoretical (using an idealized model setup), and they are all dedicated to simulating the effect that unresolved scales produce in the advection term, not in the equation of state. Yet, the problem is much more simple with the equation of state, since there is no modification in the advection/diffusion formulation, and thus no modification in the basic conservation properties of the model. The only exception is that, because of the stochastic fluctuations of $\Delta\rho$, there is a continual exchange of potential energy between the large scale flow and the unresolved scales (as described by the stochastic process, see discussion is Section 4.1). From a numerical point of view, this can produce some more numerical instability and using a smaller timestep can sometimes be required; but this has not been necessary in the experiments described below. The only important issue is thus to produce a density correction $\Delta\rho$ with realistic statistics.

(b) *Impact of temperature and salinity fluctuations on density*. With the parameterization in Eq. (16), what is expected in the first place is that, by making the fluctuations ΔT_i and ΔS_i proportional to the gradient, they will automatically adjust to be large in the main frontal regions of the ocean, where the mesoscale activity is the most intense. Second, by sampling temperature and salinity together at the same set of neighbouring points (defined by $\xi_i,\ i = 1, \ldots, p$), there is no need to explicitly specify the dependence between ΔT_i and ΔS_i; they will automatically move together as the local variations of temperature and salinity. Third, the same automatic effect of the random walk can be used to simulate a reasonable vertical structure for ΔT_i and ΔS_i, which is crucially important to reflect the vertical coherence of the mesoscale fluctuations (as observed in Fig. 2). This is why the *same* set of random walks $\xi_i,\ i = 1, \ldots, p$ will be used for all grid points of the same water column, so that the vertical variations of ΔT_i and ΔS_i in Eq. (16) will only result from the vertical variations of the large-scale gradients (∇T and ∇S). This must be understood as a first simple assumption, neglecting for instance vertical variations in unresolved lateral stirring and mixing.

On the contrary, the random walks will be generated independently for every water column, to reflect the decorrelation of the unresolved mesoscale fluctuations from one ORCA2 grid point to the next (as observed in the results of Fig. 2). It must be noted, however, that this could be easily generalized to a specified or flow-dependent horizontal correlation structure, by applying an appropriate horizontal filtering operator to the random walks: $\tilde{\xi}_i = \mathcal{F}[\xi_i]$ or by solving an elliptic equation: $\mathcal{L}[\tilde{\xi}_i] = \xi_i$ (together with the adequate amplification factor to restore the original standard deviation), Such refinements of the model will not be considered in this preliminary study.

However, what is certainly important to tune correctly in the statistical model is the shape of the probability distribution for $\Delta\rho$, which results from the superposition of several Gaussian probability distributions for ΔT_i and ΔS_i. For that purpose, it is easier to use the first-order approximation of Eq. (15), which can be written:

$$\Delta\rho = \frac{\partial^2\rho}{\partial T^2}\left(\frac{1}{2p}\sum_{i=1}^{p}\Delta T_i^2\right) + 2\frac{\partial^2\rho}{\partial T\partial S}\left(\frac{1}{2p}\sum_{i=1}^{p}\Delta T_i\Delta S_i\right) + \frac{\partial^2\rho}{\partial S^2}\left(\frac{1}{2p}\sum_{i=1}^{p}\Delta S_i^2\right) \tag{19}$$

From this equation, it is indeed immediately clear that the density correction $\Delta\rho$ is the sum of the square of Gaussian random variables (after diagonalisation to remove the cross-products). Furthermore, if these Gaussian variables are identically distributed (i.e. if all random walks have the same statistics: $\ell_{i,x} = \ell_x, \ell_{i,y} = \ell_y, \ell_{i,z} = \ell_z$, $\forall i = 1, \ldots, p$, so that $\overline{\Delta T_i^2} = \overline{\Delta T^2}$, $\overline{\Delta T_i\Delta S_i} = \overline{\Delta T\Delta S}$, $\overline{\Delta S_i^2} = \overline{\Delta S^2}$,

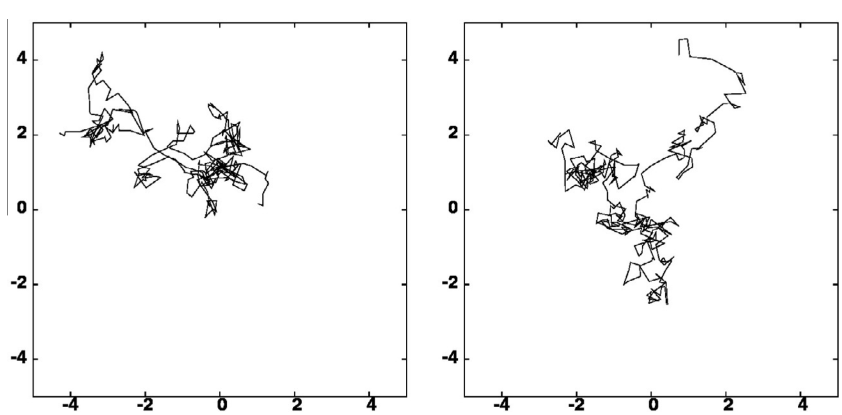

Fig. 3. Horizontal components of two random walks, as simulated during 20 days using Eq. (17), with $\ell_x = \ell_y = 2$; grid points and $\tau = 180$; time steps.The axes are labelled in number of grid points.

Table 2
Statistical parameters defining the random walks in Eq. (17). A dependence with latitude (λ) is introduced to avoid unrealistic effects and numerical instability in tropical regions.

Number of random walks	$p = 6$
Horizontal standard deviation ($i = 1, \ldots, p$)	$\ell_x = \ell_y = 4.2 \lvert \sin \lambda \rvert$ grid points
Vertical standard deviation ($i = 1, \ldots, p$)	$\ell_z = \lvert \sin \lambda \rvert$ grid points
Correlation timescale ($i = 1, \ldots, p$)	$\tau = 180$ time steps

$\forall i = 1, \ldots, p$), then $\Delta\rho$ is distributed like a chi-square distribution with p degrees of freedom (with a negative multiplicative factor, containing the factor $1/p$). And the main characteristics of the $\Delta\rho$ distribution are:

- the mean: $\overline{\Delta\rho} = \frac{1}{2}\left[\frac{\partial^2\rho}{\partial T^2}\overline{\Delta T^2} + 2\frac{\partial^2\rho}{\partial T \partial S}\overline{\Delta T \Delta S} + \frac{\partial^2\rho}{\partial S^2}\overline{\Delta S^2}\right]$
- the standard deviation: $\sigma_{\Delta\rho} = \sqrt{\frac{2}{p}}\lvert\overline{\Delta\rho}\rvert$
- the mode: $\widehat{\Delta\rho} = 0$ for $p \leqslant 2$ and $\widehat{\Delta\rho} = \frac{p-2}{p}\overline{\Delta\rho}$ for $p \geqslant 2$

Thus the mean density difference $\overline{\Delta\rho}$ does not depend on the number of degrees of freedom p in the temperature and salinity fluctuations, and the main effect of increasing p is to reduce the dispersion of $\Delta\rho$ around the mean (since the standard deviation $\sigma_{\Delta\rho}$ decreases as $1/\sqrt{p}$). Moreover, for $p \leqslant 2$, the mode of the distribution is $\Delta\rho = 0$, which means that small $\Delta\rho$ remain very probable, and would appear quite often in the time series (inconsistently with Fig. 2). On the contrary, as the number of degrees of freedom in the fluctuations increases, the probability that they are all close to zero (which is necessary for the mean square $\Delta\rho$ to be close to zero) becomes smaller and smaller, and the peak $\widehat{\Delta\rho}$ gets closer to the mean $\overline{\Delta\rho}$. (For $p \to \infty$, the distribution even becomes asymptotically Gaussian, with mean $\overline{\Delta\rho}$ and standard deviation $\sigma_{\Delta\rho}$.) This corresponds to what happens in the real ocean: the more degrees of freedom in the unresolved scales (for every ORCA2 grid point), the less probable it is that the effect of the fluctuations can almost totally disappear (i.e. $\Delta\rho$ becoming close to zero). Hence, in the parameterization of the stochastic processes, p is the parameter to tune to obtain the right dispersion of $\Delta\rho$ around the mean $\overline{\Delta\rho}$ (as observed in Fig. 2).

(c) *Density modification $\Delta\rho$ in the model.* Table 2 summarizes the statistical parameters that have been used to define the stochastic equation of state using Eqs. (15) to (18), and Fig. 4 shows the resulting density difference $\Delta\rho$ that it produces in the ORCA2 simulation (computed as the difference between Eqs. (15) and (6)). The three panels of Fig. 4 show the same three kinds of results that were obtained in Fig. 2 from the GLORYS reanalysis: (a) $\Delta\rho$ in the surface model layer for January (corresponding to the 25th year of the perpetual ORCA2 simulation), (b) $\Delta\rho$ for the vertical profile at 47.5°W 42.6°N for the same date, and (c) $\Delta\rho$ for the time series corresponding to the same location and to the same year. What we can conclude from the comparison between Figs. 2 and 4 is that the stochastic parameterization of the equation of state is qualitatively able to reproduce (i) the right horizontal pattern for $\Delta\rho$, mainly concentrated in the Western boundary currents and in the Antarctic circumpolar current (but the values are about two times larger), (ii) a reasonable vertical structure for $\Delta\rho$ (varying quite smoothly with depth, but with a sharper gradient between 200 and 500 m depth), and (iii) a fluctuating time series (with a similar annual cycle but much larger high frequency fluctuations). Because of the simplicity of the statistical model (in Table 2) and because of the

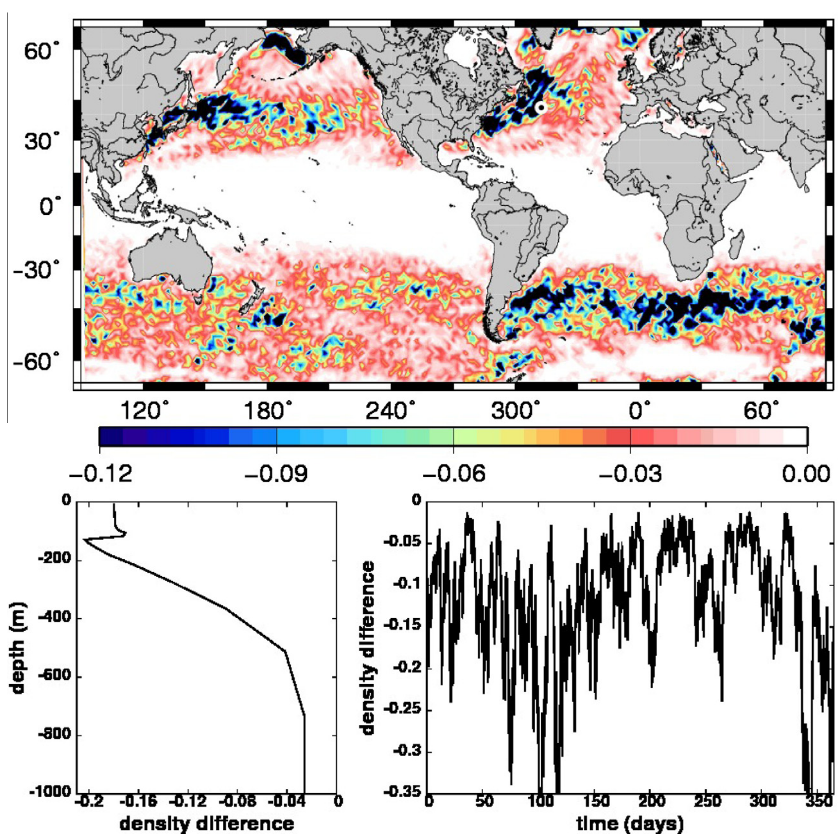

Fig. 4. Density difference $\Delta\rho$ produced by the stochastic parameterization (a) for the surface model layer on January 1, year 5 (top panel), (b) for the vertical profile at 48°W 43.2°N (the position of the black dot in the top panel) for the same date (bottom left panel), and (c) for the surface time series (corresponding to the 25th year of the perpetual simulation) at the same horizontal location (bottom right panel).

inaccuracy of the reference data (in Fig. 2), the adequation between the simulated and observed $\Delta\rho$ can only be rather approximate. On the one hand, the amplitude and pattern of $\Delta\rho$ in Fig. 4 are very sensitive to the amplitude of the stochastic fluctuations (i.e. the length scales of the random walks). If the amplitude of $\Delta\rho$ is made similar to the values obtained from the reanalysis data (in Fig. 2) by reducing the length scales listed in Table 2, then the mean flow is already strongly modified, but not quite sufficiently to make the pattern of $\Delta\rho$ similar to Fig. 2 (especially in the Gulf Stream region). On the other hand, it must be emphasized that the reanalysis data do not provide the right $\Delta\rho$, but only a lower bound. At a $1/4^\circ$ resolution, the reanalysis still misses a large part of the mesoscale fluctuations. Without high resolution observations of both temperature and salinity (in 3D), it is difficult to compute a better estimate of $\Delta\rho$. However, by comparing high resolution observations of sea surface temperature to the $1/4^\circ$ reanalysis, one can easily get convinced that a 40% overhead for ΔT and ΔS (so that $\Delta\rho$ is about twice larger) to account for the missing part of the spectrum is not particularly large. These difficulties explain why a concise qualitative comparison of typical behaviours has been preferred to a detailed quantitative comparison of the statistics of $\Delta\rho$. The improvement of the statistical model using more accurate reference data is thus left for further studies.

What is important to realize is that the $\Delta\rho$ space and time patterns illustrated in Fig. 4 have been produced, in a fully autonomous way, by the ORCA2 model simulation, without any other additional information than that included in Eqs. (15) to (18) and in Table 2. Furthermore, to produce the effect that is displayed in

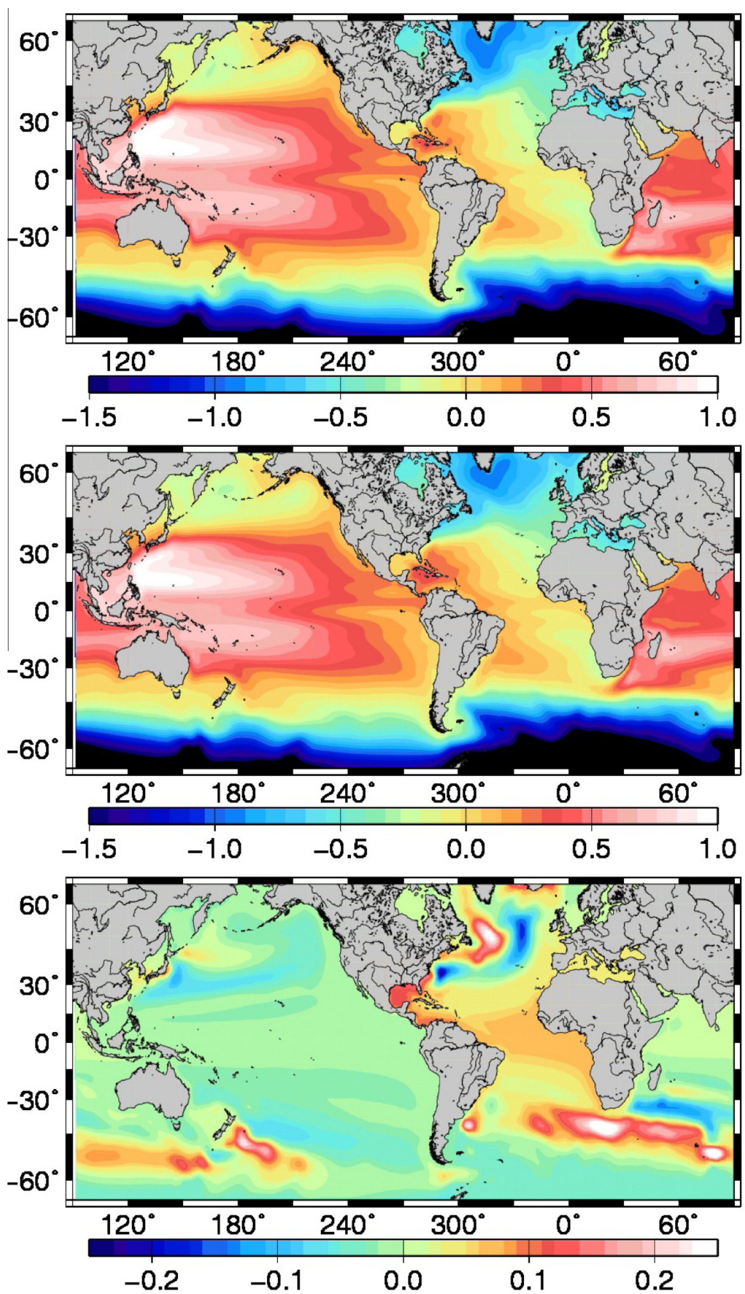

Fig. 5. Mean sea surface height (in m), as obtained (i) with the standard ORCA2 configuration (top panel), and (ii) with the stochastic parameterization of the equation of state (middle panel). The bottom panel shows the difference produced by the stochastic parameterization.

Fig. 4, the stochastic model (Eqs. (15)–(18)) and the dynamical model (Eqs. (1)–(5)) are coupled in two ways. On the one hand, the stochastic parameterization of the equation of state depends on the ocean circulation that is simulated by the model, through the temperature and salinity gradient in Eq. (16). On the other hand, the model circulation is directly influenced by the effect of the stochastic equation of state on the horizontal pressure gradient. This will be discussed in the next section.

4. Impact on the model simulation

The purpose of this section is to provide an overview of the effect that the stochastic parameterization described in Section 3 produces in the low resolution global ocean model described in Section 2. For that purpose, two model simulations will be compared: the reference simulation is performed using the standard NEMO primitive equation model, as described by Eqs. (1)–(10); and the stochastic simulation is performed by replacing the deterministic equation of state in Eq. (6) by the stochastic equation of state given by Eqs. (15)–(18).

However, it is important to remark that the stochastic simulation is essentially different from the reference simulation, in the sense that it is only one possible realization, randomly sampled from a large set of possibilities. In principle, an ensemble of simulations is thus needed to properly describe the probability distribution of the model results (reflecting the uncertainties that unresolved scales produce in the large-scale density gradient). In this study, however, one stochastic simulation will be sufficient, because only the average response to the stochastic parameterization will be considered, and because the ensemble average can be replaced by a time average. It is exactly for the same reason that it can be meaningful to look at just one eddy-resolving model simulation despite the non-deterministic nature of the eddy flow.

In the rest of the paper, all figures will represent averages over the last 10 years of the model simulations (between years 16 and 25). These averages have the same meaning in the two simulations and can thus be compared.

4.1. Global circulation

Fig. 5 shows the mean sea surface height $\langle\eta\rangle$ that is produced by the two simulations, and the difference between them. Although the general pattern is quite similar, substantial differences are produced by the stochastic parameterization, especially in the geographical locations of the main frontal zones, where the unresolved mesoscale activity is the most intense. The subtropical gyres are higher in the Atlantic and slightly lower in the Pacific, and, except in the South Atlantic, their latitudinal extension is systematically reduced. The Kuroshio (North Pacific) and the Gulf Stream (North Atlantic) pathways are moved southward (except the North West corner in the Gulf Stream extension, which is moved in the opposite direction), whereas the South Pacific and South Indian currents are moved northward. In the South Atlantic, the structure of the confluence zone is modified, with increased sea surface height at the approximate position of the Zapiola anticyclone, and the Agulhas current is extending further East towards the South Atlantic ocean. As a consequence, the subtropical gyre extends further south in the South Atlantic, and the Antarctic circumpolar front is thinner there in comparison to the reference simulation. All these modifications go towards correcting known biases in the sea surface height that is simulated by low resolution

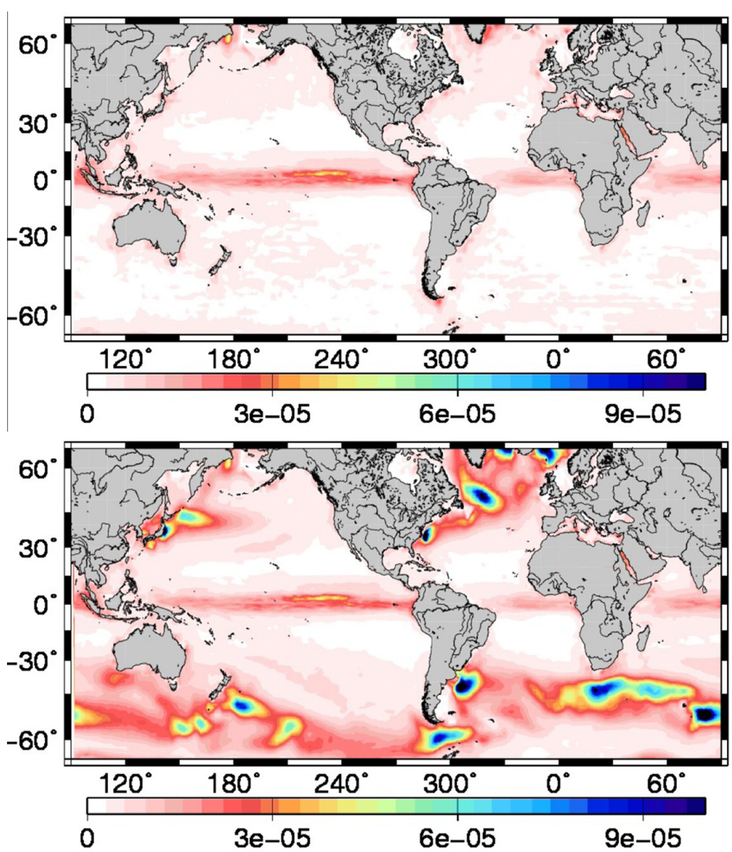

Fig. 6. Root mean square vertical velocity (in m/s, at 100 m depth), as obtained (i) with the standard ORCA2 configuration (top panel), and (ii) with the stochastic parameterization of the equation of state (bottom panel).

global ocean models, with respect to the observed dynamic height (as obtained from various sources, see Rio and Hernandez, 2004).

However, if the above results clearly show that the stochastic parameterization described in Section 3 produces a very significant impact on the model general circulation, it is certainly premature (and out of the scope of this study) to try validating the results against observations, mainly because the stochastic simulation is very sensitive to the statistical parameters listed in Table 2. It is too sensitive indeed to consider that the statistical model is fully validated by the simple comparison between Figs. 2 and 4. First, according to Eq. (19), the density difference $\Delta\rho$ is proportional to the square of the temperature and salinity fluctuations, and thus to the square of the length scales $\ell_{x,i}, \ell_{y,i}, \ell_{z,i}$ of the random walks. Hence, these length scales do not need to be very different to substantially modify $\Delta\rho$ and the resulting model general circulation. Second, the stochastic fluctuations of $\Delta\rho$ (governed by the number p of random walks and by the timescales τ_i) also produce a decisive impact on the mean circulation. Without fluctuations of $\Delta\rho$ ($p \to \infty$ or $\tau \to \infty$), mimicking the stochastic forcing of the unresolved scales on the large-scale density, the pathway of the main current cannot be modified in the same way, which leaves little hope of reproducing the same kind of mean behaviour with a non-stochastic parameterization of $\Delta\rho$. Here, the underlying phenomenon (presumably largely underestimated in the GLORYS data in Fig. 2) is that, because of the nonlinearity of the equation of state, the unresolved scales produce *high frequency* fluctuations of the large scale density, which need to be simulated in the low resolution model. For these reasons, it is of key importance that the statistics of $\Delta\rho$ can be further validated using either real world observations or high resolution ocean models.

At this stage, it is nonetheless useful to study the consequences of the fluctuations of $\Delta\rho$ in the model simulation. Because of the nonlinearity of the equation of state, the unresolved scales produce unknown fluctuations of the large scale density, which corresponds to a continual exchange of potential energy between the unresolved scales and the large scales. In the real ocean, the potential energy of the large-scale flow is thus constantly re-structured by a flux of information from the smaller scales. In the stochastic parameterization, the missing information is provided by the random numbers in Eq. (17), which produce (through Eq. (16), and then Eq. (15)) a continual re-organization of the large-scale density field. Because of this, the large-scale flow is constantly further away from geostrophic equilibrium (compared to the reference simulation), so that the instationary and advection terms play a larger role in Eq. (1). Moreover, this continual and never ending adjustment of the model to geostrophy generates much higher associated vertical velocities, as illustrated in Fig. 6. In the figure, it can be seen that high vertical velocities (up to $\sim 10^{-4}$ m/s RMS) are generated in the regions where the density fluctuations are greatest (as shown in Fig. 4). Such high vertical velocities (associated with the large scales) in the mid-latitudes were totally absent in the reference simulation, and their magnitude is obviously also very sensitive to the stochastic parameterization of the density fluctuations. Since the amplitude of these fluctuations is difficult to evaluate accurately with available data, the magnitude of these additional vertical velocities should also be considered with care.

This means that uncertainties in the stochastic parameterization of uncertainties can directly produce uncertainties in the model itself (here in the vertical advection). Hence, an approximation

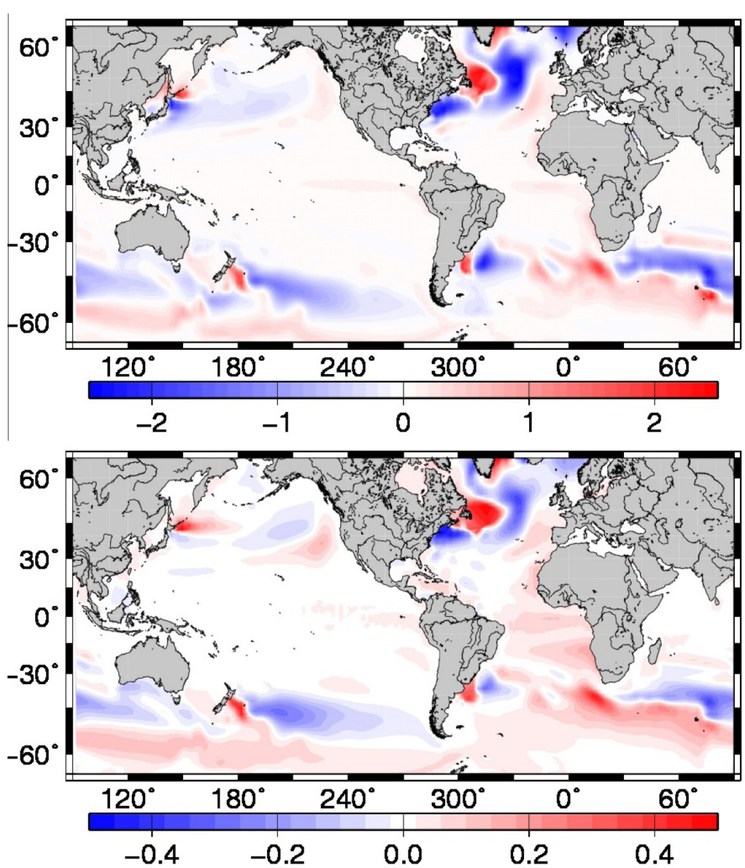

Fig. 7. Mean sea surface temperature difference (in degree Celsius, top panel), and sea surface salinity difference (bottom panel) produced by the stochastic parameterization of the equation of state.

must be found to close the parameterization somewhere (here a simple closure is defined by the parameters in Table 2). On the other hand, as a perspective, the diagnostic of the vertical velocities could in turn be used to design a stochastic parameterization of the hydrostatic approximation in Eq. (2). However, it is clear that this modelling effort cannot be continued indefinitely, and that an appropriate approximation must be found to obtain the right model complexity, including all relevant processes and uncertainties, and providing a bulk parameterization for all remaining uncertainties.

4.2. Air–sea interactions

One of the most important effect of the change in the average model circulation is to strongly modify the distribution of heat and salt in the ocean, and thus to modify the interaction with the atmosphere. Fig. 7 shows for instance the mean sea surface temperature and salinity difference between the stochastic and the reference simulations. As can be expected from the modification in the mean surface circulation illustrated in Fig. 5, the main differences occur along the fronts separating the subtropical and subpolar gyres. The largest mean difference occurs in the Gulf Stream region, where it can reach about 5 °C and 1 psu. Again, these modifications go towards correcting the largest known temperature and salinity biases in low resolution ocean models, as compared to observations.

In addition, this change in the redistribution of heat in the ocean has a considerable effect in the interaction with the atmosphere. In forced ocean models, with prescribed atmospheric conditions (see Table 1), a strong bias in the sea surface temperature is inconsis-

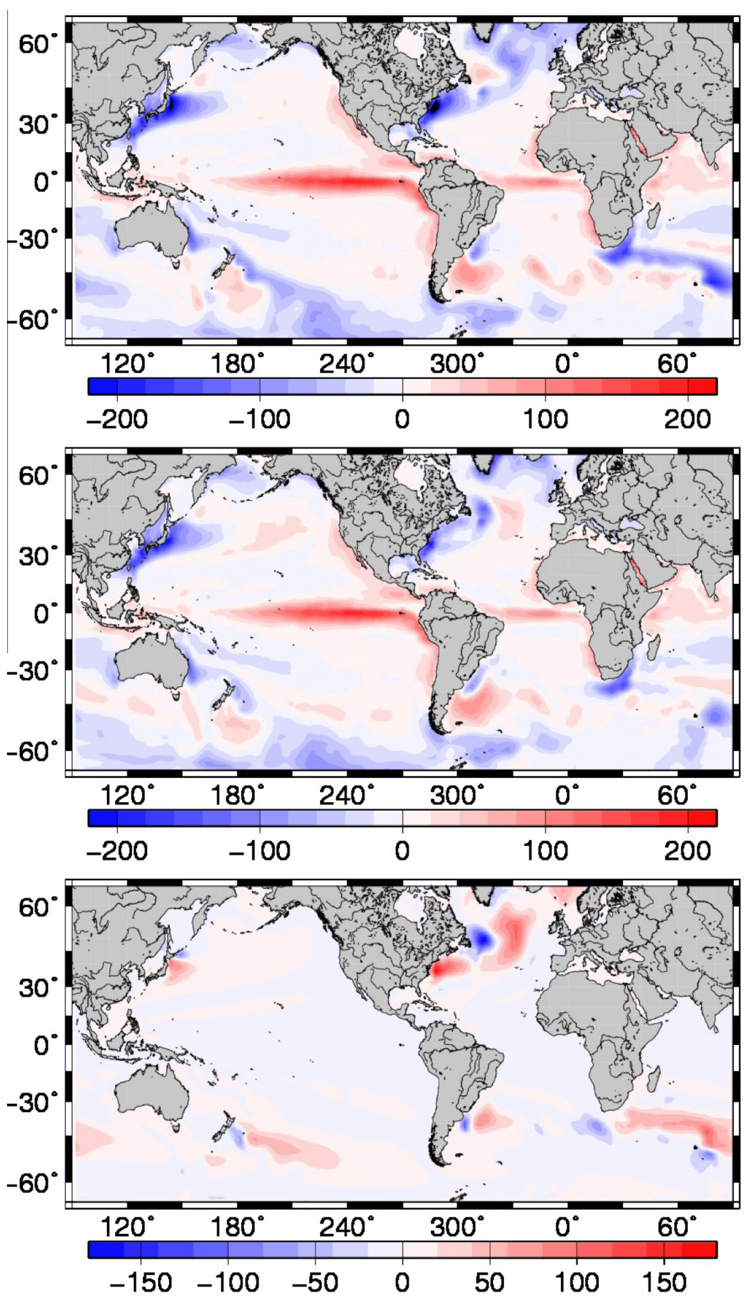

Fig. 8. Mean net air–sea heat flux (in W/m^2), as obtained (i) with the standard ORCA2 configuration (top panel), and (ii) with the stochastic parameterization of the equation of state (bottom panel). The bottom panel shows the difference produced by the stochastic parameterization.

tent with the atmosphere, which is realistic, and the forcing formulation reacts by producing a spurious heat flux, which can be extremely unrealistic. For instance, in the Gulf Stream region, if warm waters are advected too far north by a bias in the circulation, they will meet a very cold atmosphere, and a very strongly negative heat flux will result (down to about $-250\ \mathrm{W/m^2}$ in average). This effect on the average net heat flux is illustrated in Fig. 8, showing that it is particularly important in the Gulf Stream and Kuroshio regions in the reference simulation, whereas it is very strongly reduced in the stochastic simulation. Zonal patterns of negative flux in the Southern Ocean can also be observed in the reference simulation (South East of New-Zealand and South East of South-Africa). The absence of these patterns in the stochastic simulation is a clear indication that the position of the fronts has been improved, since it is in better agreement with the atmospheric data. In coupled models, such as climate models, which are currently constructed with a low resolution ocean component, the situation is not better, since the bias in the ocean circulation propagates to the atmosphere. As a result, the uncertainties in the large-scale density associated to the nonlinearity of the equation of state for sea water can have a significant impact on the simulated earth's climate. This particular effect is thus also a good example or the importance of faithfully simulating model uncertainties in climate studies (as already pointed out for instance in the works of Berner et al. (in press), Williams (2012)).

5. Conclusions

In this study, it has been shown (i) that, as a result of the nonlinearity of the seawater equation of state, unresolved scales represent a major source of uncertainties in the computation of the large-scale horizontal density gradient from the large-scale temperature and salinity fields, and (ii) that the effect of these uncertainties can be simulated using random processes to represent unresolved temperature and salinity fluctuations. However, the stochastic parameterization of the uncertainties still suffers from several shortcomings and approximations, as for instance the use of random walks with zonally uniform statistical properties, uncorrelated on the horizontal and fully correlated along the vertical. This is why further improvement and validation of the statistical model are certainly needed to better quantify the magnitude of this effect.

The results of experiments performed with a low resolution global ocean model show that this parameterization produces a considerable effect on the average large-scale circulation of the ocean, especially in the regions of intense mesoscale activity (like the Western boundary current and the Antarctic circumpolar current). The large-scale flow is less geostrophic, with more intense associated vertical velocities, and the average geographical position of the main temperature and salinity fronts is more consistent with the observations. In particular, the simulations suggest that the stochastic effect of the unresolved temperature and salinity fluctuations on the large-scale density may be sufficient to explain why the Gulf Stream pathway systematically overshoots in non-stochastic low resolution ocean models.

More generally, this study supports the idea that the explicit simulation of uncertainties by stochastic parameterizations is needed to eliminate biases in ocean models (Palmer, 2012). This is singularly important in climate applications, for which it is more important for the model to be unbiased than accurate (i.e. to produce the right attractor rather than accurate instantaneous tendencies). This is also the natural way of producing the probabilistic forecasts that are required to objectively validate model results against observations (or to solve inverse problems). Hence, because the cost of simulations is always a constraint to the modeller, an appropriate tradeoff should always be sought between resolving more phenomena and more scales (hopefully increasing model accuracy), and explicitly simulating uncertainty using a large ensemble forecast (hopefully reducing simulation biases and increasing the statistical significance of the results).

6. Acknowledgements

This work was conducted as a contribution to the SANGOMA project funded by the E.U. (grant FP7-SPACE-2011-1-CT-283580-SANGOMA), with additional support from CNES. I wish to thank Jacques Verron and Pierre Brasseur for their support to this study and for their encouragements to publish this work; and I am also grateful to the anonymous reviewers for their useful comments and suggestions. The calculations were performed using HPC resources from GENCI-IDRIS (Grant 2011-011279).

References

Barnier, B., Madec, G., Penduff, T., Molines, J., Tréguier, A., Beckmann, A., Biastoch, A., Boning, C., Dengg, J., Gulev, S., Le Sommer, J., Rémy, E., Talandier, C., Theetten, S., Maltrud, M., Mc Lean, J., 2006. Impact of partial steps and momentum advection schemes in a global ocean circulation model at eddy permitting resolution. Ocean Dyn. 56 (5–6), 543–567.

Berloff, P.S., 2005. On rectification of randomly forced flows. J. Marine Res. 63 (3), 497–527.

Berner, J., Jung, T., Palmer, N., in press. Systematic model error: the impact of increased horizontal resolution versus improved stochastic and deterministic parameterizations, J. Climate. http://dx.doi.org/10.1175/JCLI-D-11-00297.1.

Blanke, B., Delecluse, P., 1993. Low frequency variability of the tropical atlantic ocean simulated by a general circulation model with mixed layer physics. J. Phys. Oceanograph. 23, 1363–1388.

Bryan, K., Lewis, J., 1979. A water mass model of the global ocean. J. Geophys. Res. 84 (C5), 2503–2517.

Buizza, R., Miller, M., Palmer, T.N., 1999. Stochastic representation of model uncertainties in the ECMWF ensemble prediction system. Quater. J. Royal Meteorol. Soc. 125, 2887–2908.

Emile-Geay, J., Madec, G., 2009. Geothermal heating, diapycnal mixing and the abyssal circulation. Ocean Sci. 5, 281–325.

Evensen, G., 1994. Sequential data assimilation with a nonlinear quasi-geostrophic model using Monte Carlo methods to forecast error statistics. J. Geophys. Res. 99 (C5), 10143–10162.

Ferry, N., Parent, L., Garric, G., Barnier, B., Jourdain, N., 2010. The Mercator ocean team, Mercator global eddy permitting ocean reanalysis GLORYS1V1: description and results. Mercator Ocean Newslett. 36, 15–27.

Frederiksen, J., O'Kane, T., Zidikheri, M., 2012. Stochastic subgrid parameterizations for atmospheric and oceanic flows. Phys. Scripta 85, 068202. http://dx.doi.org/10.1088/0031-8949/85/06/068202.

Griffies, S.M., Böning, C., Bryan, F., Chassignet, E.P., Gerdes, R., Hasumi, H., Hirst, A., Treguier, A.-M., Webb, D., 2000. Developments in ocean climate modelling. Ocean Modell. 2 (3–4), 123–192.

Jackett, D.R., McDougall, T.J., 1995. Minimal adjustment of hydrographic data to achieve static stability. J. Atmos. Oceanic Technol. 12, 381–389.

Kazantsev, E., Sommeria, J., Verron, J., 1998. Subgrid-scale eddy parameterization by statistical mechanics in a barotropic ocean model. J. Phys. Oceanograph. 28, 1017–1042.

Klocker, A., McDougall, T.J., 2010. Influence of the nonlinear equation of state on global estimates of dianeutral advection and diffusion. J. Phys. Oceanograph. 40, 1690–1709.

Large, W., Yeager, S., 2009. The global climatology of an interannually varying air–sea flux data set. Climate Dyn. 33, 341–364.

Levitus, S. et al., 1998. World ocean database 1998, Atlas NESDIS 18, NOAA.

Madec, G., 2008. The NEMO team, NEMO ocean engine, Note du Pôle de modélisation 27. Institut Pierre-Simon Laplace (IPSL), France, ISSN 1288-1619.

Madec, G., Imbard, M., 1996. A global ocean mesh to overcome the north pole singularity. Climate Dyn. 12, 381–388.

McDougall, T.J., McIntosh, P.C., 1996. The temporal-residual-mean velocity. Part I: Derivation and the scalar conservation equations. J. Phys. Oceanograph. 26, 2653–2665.

McDougall, T.J., McIntosh, P.C., 2001. The temporal-residual-mean velocity. Part II: Isopycnal interpretation and the tracer and momentum equations. J. Phys. Oceanograph. 31, 1222–1246.

Palmer, T., 2012. Towards the probabilistic Earth-system simulator: a vision for the future of climate and weather prediction. Q. J. R. Meteorol. Soc. 138, 841–861.

Palmer, T., Shutts, G., Hagedorn, R., Doblas-Reyes, F., Jung, T., Leutbecher, M., 2005. Representing model uncertainty in weather and climate prediction. Annu. Rev. Earth Planet. Sci. 33, 163–193.

Penduff, T., Juza, M., Brodeau, L., Smith, G., Barnier, B., Molines, T.A.-M., Madec, J.-M., G., 2010. Impact of global ocean model resolution on sea-level variability with emphasis on interannual time scales. Ocean Sci. 6, 269–284.

Rio, M., Hernandez, F., 2004. A mean dynamic topography computed over the world ocean from altimetry, in situ measurements, and a geoid model. J. Geophys. Res. 109, C12032. http://dx.doi.org/10.1029/2003JC002226.

Roullet, G., Madec, G., 2000. Salt conservation, free surface, and varying levels: a new formulation for ocean general circulation models. J. Geophys. Res. 105, 23927–23942.

The DRAKKAR Group, 2007. Eddy-permitting ocean circulation hindcasts of past decades. CLIVAR Exchang. 42 12 (3), 8–10.

UNESCO, 1983. Algorithms for computation of fundamental property of sea water, Techn. Paper Mar. Sci. 44 UNESCO.

Van Kampen, N.G., 2007. Stochastic Processes in Physics and Chemistry. Elsevier, p. 463..

Williams, P.D., 2012. Climatic impacts of stochastic fluctuations in air–sea fluxes. Geophys. Res. Lett. 39, L10705. http://dx.doi.org/10.1029/2012GL051813.

Zhai, X., Greatbatch, R.J., Sheng, J., 2004. Diagnosing the role of eddies in driving the circulation of the northwest Atlantic Ocean. Geophys. Res. Lett. 31, 1–4.

Zidikheri, M., Frederiksen, J., 2010. Stochastic modelling of unresolved eddy fluxes. Geophys. Astrophys. Fluid Dyn. 104, 323–348.